ACS APPLIED MATERIALS & INTERFACES

Research Article

www.acsami.org

Core (Polystyrene)−Shell [Poly(glycerol monomethacrylate)] Particles

Andrew Mckenzie,[†] Richard Hoskins,[‡] Thomas Swift,[‡] Colin Grant,[§] and Stephen Rimmer*[,‡]

[‡]School of Chemistry and Biosciences, University of Bradford, Bradford, West Yorkshire BD7 1DP, U.K.

[§]Department of Engineering, University of Bradford, Bradford, West Yorkshire BD7 1DP, U.K.

[†]Department of Chemistry, University of Sheffield, Sheffield, South Yorkshire S3 7HF, U.K.

Supporting Information

ABSTRACT: A set of water-swollen core−shell particles was synthesized by emulsion polymerization of a 1,3-dioxolane functional monomer in water. After removal of the 1,3-dioxolane group, the particles' shells were shown to swell in aqueous media. Upon hydrolysis, the particles increased in size from around 70 to 100−130 nm. A bicinchoninic acid assay and ζ-potential measurements were used to investigate the adsorption of lysozyme, albumin, or fibrinogen. Each of the core−shell particles adsorbed significantly less protein than the noncoated core (polystyrene) particles. Differences were observed as both the amount of difunctional, cross-linking monomer and the amount of shell monomer in the feed were changed. The core−shell particles were shown to be resistant to protein adsorption, and the degree to which the three proteins adsorbed was dependent on the formulation of the shell.

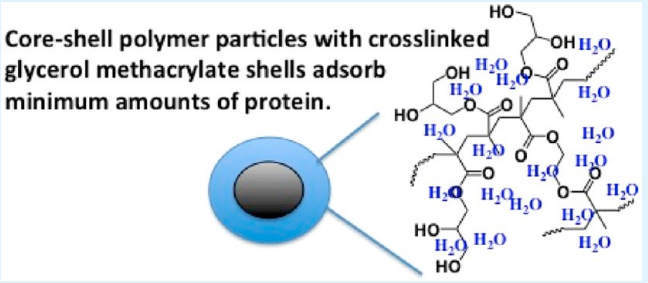

KEYWORDS: *core−shell, particles, emulsion polymerization, hydrogel, protein adsorption*

INTRODUCTION

Core−shell (CS) particles are materials with layered multidomain morphologies in which the layers have different compositions. Particles of this type have found a large number of uses in a wide variety of applications. Targeting drugs with polymers is an important aspect of medicine that promises advanced therapies.[1] However, targeting also requires avoiding the immune system, and protein adsorption is typically the first event that begins the multiple features of the immune response. CS particles are useful in drug delivery. For example, an antiinflammatory peptide was released from CS microparticles with polylactide cores and a hydrogel shell formed from chitosan and alginate.[2] CS particles with inorganic cores and polymer shells are also attracting interest.[3] The release of growth factors from polymer particles is an important route to controlling the delivery of these often charged cytokines. Lim et al. showed the sustained delivery of two important heparin binding growth factors for up to 21 days from a heparin/chitosan composite particle,[4] and later Platt et al. showed how the release rates could be controlled by delivery from sulfate functional CS polymer particles with poly(acrylamide 2-methylpropanesulfonate) shells.[5] Chatterjee et al. reviewed the use of CS particles and other nanoparticles in medicine,[6] and Goldberg et al. provided an extensive review of the potential uses of nanoparticles in a range of medical technologies.[7] Hydrogel particles that deswell in response to stimuli have potential in controlled release mediated by changes in the external environment.[8,9] Block copolymer micelles have CS structure, and these particles have been used for a number of delivery applications,[10] including the delivery of DNA.[11] CS particles have also been used as vehicles for sensors and diagnostics: for monitoring of the pH,[12] for the detection of atrazine,[13] for the removal of lead,[14] as a sensor for hydrogen sulfide,[15] or for detection of the H5N1 influenza virus using metal-enhanced fluorescence.[16]

There are also large numbers of examples in the literature that highlight the usefulness of exploiting the magnetic properties of some types of particles, for example, as a means of virus-free gene delivery,[17] targeted drug delivery,[18] or easy separation and collection of the particles when their intended role had been completed, such as when used as a catalyst.[19]

However, the synthesis of particles with aqueous swollen shells (hydrogel shells) and hydrophobic cores is very difficult if water-soluble monomers are used, even when polyfunctional cross-linking comonomers are used.[20] The difficulty arises because the hydrophilic monomers tend to polymerize in the aqueous phase and do not form a shell on the existing core particles. Strategies to provide such CS particles include polymerization with amphiphilic macromonomers at the shell stage,[21] adsorption of shell monomers with opposite charge onto the cores and in situ polymerization,[22] and simple encapsulation of a porous core in the shell.[23] Another

Received: November 22, 2016
Accepted: February 13, 2017
Published: February 13, 2017

DOI: 10.1021/acsami.6b15004
ACS Appl. Mater. Interfaces 2017, 9, 7577−7590

possibility is to use a hydrophilic macroinitiator and macrotransfer agents.[24−26] In some cases, it is possible to use the monomer reactivity ratios in emulsion polymerization to produce blocklike copolymers that organize into CS structures in water.[27−30] An alternative that can be applied to some monomers is to polymerize a hydrophobic monomer that can be converted to hydrophilic repeat units after polymerization. This approach has been used to produce particles with polystryene and *N*-acetylglucosamine methacrylate shells via copolymerization of a hydrophobically modified 5-acetamido-2-(acetoxymethyl)-6-[2-(methacryloyloxy)ethoxy]tetrahydro-2*H*-pyran-3,4-diyl diacetate glucosamine monomer.[31] Here we show a similar technique in which polymerization of a monomer, containing a 1,3-dioxolane group, in the second step of a sequential emulsion polymerization is followed by hydrolysis to yield a shell containing 1,2-diol functional monomer repeat units.

Many of the applications of CS particles involve contact with biological fluids. Therefore, the development of particles with shells that are resistant to the nonspecific adsorption of proteins can provide stealth particles that are proposed for delivery. However, a much more detailed study of the effects of architecture and structure is required before such materials become useful in clinical applications.[32−34] Many of the particles that are in widespread use have poly(ethylene glycol) surfaces, but other hydrogel polymers are also known to be protein-resistant; for example, noncharged monomers are used commercially in contact lenses, and hydrogels prepared from such monomers appear to be relatively resistant to fouling with proteins.[35] In this respect, we have shown that hydrogels based on polymers of 2,3-propanediol-1-monomethacrylate [glycerol methacrylate (GMA)], which is also of use in contact lens manufacturing, are relatively resistant to nonspecific protein adsorption,[36,37] do not support cell adhesion (unless modified with hydrophobes,[36,37] alkyl amines,[46,47,38,39] or cell adhesive peptides[48,40]), and do not activate macrophages.[41] Other work on GMA polymers also has shown that poly(GMA) (PGMA) amine derivatives can provide less toxic transfection agents than other amino functional polymers.[42] Also, micelle-forming block copolymers and grafted surfaces incorporating GMA appear also to be nonfouling and non-cell-adhesive.[43,44] However, cross-linking of PGMA adds another feature to their formulation, which is expected to effect their biological performance.[36,37] Therefore, with these aspects in mind, it seems reasonable to investigate the provision of CS particles with cross-linked PGMA shells and to examine the protein adsorption properties of these materials. Our strategy involved polymerization of a GMA 1,3-dioxolane derivative in which the diol group was modified by formation of the hydrophobic 1,3-dioxolane group. This monomer (glycerol methacrylate 1,3-dioxolane, GMAc) and hydrolysis of its polymers to provide PGMA were introduced by Beinert et al.,[45] and its polymerization was further studied by Mori et al.[46] Block copolymers have also been formed with poly(GMAc) (PGMAc) segments that were hydroloyzed postpolymerization to provide amphiphilic block copolymers that formed micelles.[47,48] GMAc was used by us previously to form amphiphilic conetworks that swelled in water after 1,3-dioxolane was hydrolyzed.[37] Modification of the diol group to the hydrophobic 1,3-dioxolane provides a monomer that can be polymerized by conventional emulsion polymerization, providing core particles with PGMA shells in only two steps: sequential emulsion polymerization followed by removal of the 1,3-dioxolane group.

Zhang et al. produced block copolymer micelles with PGMAc that could be hydrolyzed to PGMA.[49] Branched block copolymer CS particles containing PGMA were also produced by us by chain-extending highly branched poly(*N*-isopropylacrylamide)s, produced by self-condensing reversible addition−fragmentation chain-transfer (RAFT) polymerization directly with GMA.[50] RAFT polymerizations were used to provide graft shells of PGMA on polystyrene or poly(hydroxypropyl methacrylamide) cores by copolymerizing PGMA macromonomers.[51] PGMA block copolymers were also used to provide other micellar polymer particles[51,43,52−56] including other shell cross-linked particles.[57,58]

Following this previous work, we considered that CS particles with hydrogel (PGMA) shells could also be produced by polymerizing hydrophobic derivatives of GMA, onto hydrophobic cores, followed by conversion of the hydrophobic derivative to the fully hydrophilic, PGMA derivative. Provided that it was cross-linked, swelling would not lead to removal of the shell by its dissolution, and cross-linking could be easily achieved by copolymerization with a difunctional monomer, such as ethanediol dimethacrylate. The approach reported here uses conventional emulsion polymerizations that are followed by acidic workups to convert the hydrophobic shell into a hydrophilic, swellable hydrogel. Few examples of similar strategies are available in the literature, but recently Suzuki et al. reported the synthesis of multilayered microgel particles using the sequential emulsion polymerizations of glycidyl methacrylate (GME, the hydrophobic epoxidized derivative of GMA) and poly(*N*-isopropylacrylamide).[59] Also, hydrolysis of poly(GME) (PGME) can be used to produce PGMA polymers of use in drug delivery.[60]

EXPERIMENTAL SECTION

Materials. Dichloromethane (DCM) and toluene were obtained from a Grubbs dry solvent system, and anhydrous pyridine, methacrylic anhydride (MA) solketal, and Amberlite 402 resin were obtained from Sigma Ltd. Deionized and distilled water were used throughout and obtained using a Millipore Direct Q ultrapurification system; water was produced with a resistance of 18 mΩ cm^{-1}. (Dimethylamino)pyridine (DMAP) was used as received from Sigma Ltd. Styrene, potassium carbonate, potassium persulfate, sodium dodecyl sulfate (SDS), and ethanediol dimethacrylate (EDMA) were obtained from Sigma and used without further purification. Divinylbenzene (DVB; Sigma) was cleaned with 5% sodium hydroxide (NaOH; 3 × 100 cm^3) prior to polymerization to remove the storage stabilizer and washed with deionized water (3 × 300 cm^3) before drying over magnesium sulfate.

Protein adsorption measurements were performed in ultrapure water. Lysozyme (Lys), fibrinogen (Fib), and albumin (Alb) were obtained from Sigma and used without further purification. Potassium chloride (KCl) was obtained from Sigma. Servapore dialysis tubing was obtained from Fisher Scientific and had a molecular weight cutoff range of 12000−14000 g mol^{-1}. Mass spectrometry was carried out by the direct infusion of a sample [diluted in methanol to 10 μg mL^{-1}, with ammonium acetate added to diminish the adducts (2 μg mL^{-1})] to a mass spectrometer (Micromass Quattro LC) using a Harvard syringe pump set at 10 μL min^{-1}. The data were acquired using a positive-mode electrospray ionization (ESI^+) ion source. Raw spectra can be found in the Supporting Information.

Synthesis of Dihydroxypropane-1-methacrylate 1,3-Dioxolane (Glycerol Methacrylate 1,3-Dioxolane, GMAc). GMAc was synthesized as reported previously.[36] Solketal (66.08 g) was dried by azeotropic distillation with dry toluene at 70 °C using a rotary evaporator. Dry solketal, dry pyridine (63.28 g), and dry DCM (500 mL) were mixed in a three-necked round-bottom flask in an ice bath with a stirrer bar, a nitrogen inlet, and a reflux condenser. DMAP (6.08

DOI: 10.1021/acsami.6b15004
ACS Appl. Mater. Interfaces 2017, 9, 7577−7590

g, 0.05 mol) was added to the reaction vessel and dissolved with stirring, and MA (92.49 g) was added dropwise under nitrogen. When the addition was completed, the reaction temperature was raised to room temperature and the vessel was stirred for 24 h. Finally, water (250 cm^3) was added to quench the reaction. The organic phase was washed with water (3 × 300 cm^3) and concentrated using a rotary evaporator. A gel-type basic anion-exchange resin was used to remove the byproduct, acrylic acid, from the concentrated liquid. Amberlite IRA 402 resin was activated by treatment with 1.0 M NaOH for 2−4 h, then repeatedly washed with water and then acetone, and added to the concentrated crude liquid GMAc. The mixture was shaken gently for 2−4 h before being filtered, and fresh activated resin was added again for 2−4 h. The liquid was distilled and the product collected at 60−70 °C under a reduced pressure of approximately 1 mmHg. Typical yield: 66 g, 66% based on solketal. ^{1}H NMR (DMSO-*d*): δ 1.28, 1.35 (2s, O(O)CCH_3), 1.89 (s CH_3C=CH_2), 3.74 (m CHCH_2O), 4.10 (m, OCH_2CH), 4.25 (m, OCH_2CH), 4.35 (q, CH(H)=CH_3), 5.60 (d CH(H)=CH_2). MS (ESI). Calcd: m/z 201.1 (MH^+). Found: m/z 146.2.

Polymerization. Batch polymerizations were conducted in a 1.0 L jacketed glass reaction vessel (Radleys, Walden, U.K.), which was equipped with a mechanical stirrer, a nitrogen inlet, a reflux condenser, and a temperature probe. To produce the cores, a typical reaction was as follows: water (100 g), SDS (1.6 g), and potassium carbonate (0.33 g) were charged to the vessel. The mixture was deoxygenated by bubbling under nitrogen with agitation for 1 h, while hot water was circulated through the jacket of the vessel to maintain the temperature of the mixture at 70 °C. After this, styrene (25 g) and DVB (3.25 g) were slowly added dropwise to the reaction; when the addition was completed, potassium persulfate (0.25g) was added to water (5 cm^3), and the mixture was stirred for 3 h. In the second (shell-forming) stage, GMAc and EDMA were mixed and added dropwise to the reaction, and the mixture was stirred for a further 3 h at 70 °C. At the end of 3 h, the temperature was raised to 80 °C for 1 h to ensure total monomer conversion. The latex was discharged from the vessel and stored at room temperature.

Particles with different shell compositions were prepared. The quantities of GMAc were 5, 10, and 15 mol % with respect to the molar quantity of styrene to create three particles with varying shell monomer concentrations. Also, particles with shells composed of 5, 10, and 15 mol % EDMA with respect to the molar quantity of GMAc, giving particles with varying shell cross-linking densities, were produced. The set of preparations with differing shell monomer concentrations had the same cross-linking composition (5 mol %). In the second set, in which the amount of EDMA was changed, the amount of GMAc was maintained at 5 mol %.

Removal of 1,3-Dioxolane Groups. A sample of the CS latex particles (25 cm^3) was added to hydrochloric acid (HCl; 0.1 or 1.0 mol dm^{-3}, 100 mL) and heated to 60 °C in a water bath for 4−8 h.

Analysis of the Latex. The ζ potentials of the latexes were obtained using a Brookhaven ZetaPals instrument at pH 7.2 at 25 °C (n = 3). The particle sizes were measured via dynamic light scattering (DLS) on a Malvern Nanoseries Nano-ZS instrument using dilute solutions (1/1000 dilution in ultrapure water) with quartz cuvettes set at 25 °C (n = 5). Fourier transform infrared (FTIR) spectroscopy measurements were carried out on a PerkinElmer FTIR spectrometer in the 4000−500 cm^3 range. Samples were dried and scraped onto an attenuated-reflectance probe. The solid content was determined by weighing the suspensions (10 mL) in a preweighed sample tube and drying the polymer samples at 60 °C until they reached a constant weight (n = 2). Samples for transmission electron microscopy (TEM) were prepared by diluting samples to a $^1/_5$ dilution in ultrapure water and adding 1 droplet to an Agar Scientific 400 mesh copper plate. This was allowed to dry for 10 min before dipping in ultrapure water to clean. The particles were stained with a 1% uranyl acetate solution and left to dry overnight prior to measurement. TEM measurements were carried out on a JEOL Jem 1200 EX MKII microscope with a tungsten filament at 60−80 kV acceleration. The resolution was 14 and 0.3 nm point to point. Samples were mounted on a holey carbon film and imaged using a Gratin camera above the photoluminescence film stage.

Atomic Force Microscopy (AFM) Data and Analysis. Dispersions of particles were diluted by 1000, and a droplet (50 μL) was placed in the center of a microscope slide. The droplet was covered and was allowed to evaporate, depositing and adhering the particles to the slide. Slides were then placed on an Asylum Research MFP-3D (Santa Barbara, CA) atomic force microscope for image analysis. An Olympus AC160 cantilever was used ($k \sim 40$ N m^{-1}; $f \sim$ 260 kHz) for all tapping-mode imaging.

A mask was applied to the baseline surface (glass substrate), and individual particles greater than this were extracted to obtain the maximum height of each particle on every image. The mean particle heights and standard error of mean values are quoted in this manuscript. Further information and all images are shown in the Supporting Information. After a region of interest was found, a 512 × 512 pixel image of the particles on the glass surface was captured. Particle heights were then isolated from the glass substrate background and extracted using the IGOR Pro data analysis software (WaveMetrics, Lake Oswego, OR). Here, we assumed that the particles are spherical and used the image particle heights to determine the particle size. AFM images of rounded objects as scanned by a parabolic-shaped probe will contain artifacts, which makes the particle widths much larger than they actually are; however, the particle heights are an accurate representation, as shown in Figure 1.

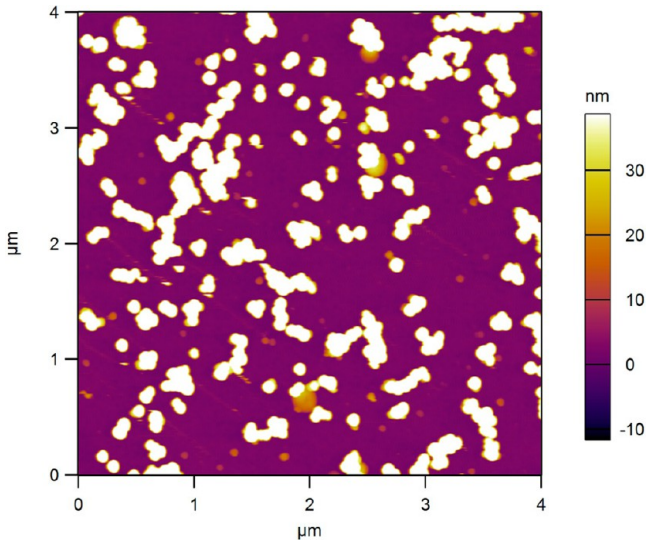

Figure 1. AFM image (4 μm height) of core (PS + DVB) particles dried on a glass plate.

Purification of the Latexes. The deprotected dispersions were centrifuged and resuspended in aqueous KCl (1.0 mmol dm^{-3}) to wash out the acid used for deprotection. Multiple washes were required (3−5) to fully wash out all of the acid and to reach the pH of KCl(aq) (approximately pH 7.2). When the particles were washed, they were stirred with activated Amberlite 402 resin to remove surfactant molecules bound to the surface from the emulsion polymerization steps. Again multiple extractions with the resin were required, and the dispersions were stirred for approximately 4 h at each wash. Following washing with the resin, the particles were filtered to remove the resin and again washed with KCl. The dispersions were then dialyzed in ultrapure water to remove any remaining surfactant. Dialysis took place over 3−5 days, with the water changed daily. Successful removal was confirmed by the observation of no change in the ζ potentials after dialysis was continued.

Protein Adsorption. The protein solutions were made in the following quantities: 50, 25, 10, 5, and 1 mg cm^{-3} in ultrapure water.

Following the successful washing and removal of surfactant, the bulk solid contents of the latexes were determined by solvent evaporation, and the latex concentration was adjusted to 10 mg cm^{-3}. Samples (1 cm^3) of the latex were taken, pipetted into Eppendorf tubes, and then

DOI: 10.1021/acsami.6b15004
ACS Appl. Mater. Interfaces 2017, 9, 7577−7590

Scheme 1. Preparation of CS Particles with Core [Poly(styrene-*co*-DVB)]−Shell [Poly(GMAc-*co*-EDMA)] Morphologies and Hydrolysis of the Shell To Give the Core−Shell Poly(styrene-*co*-DVB)−Poly(GMA-*co*-EDMA)

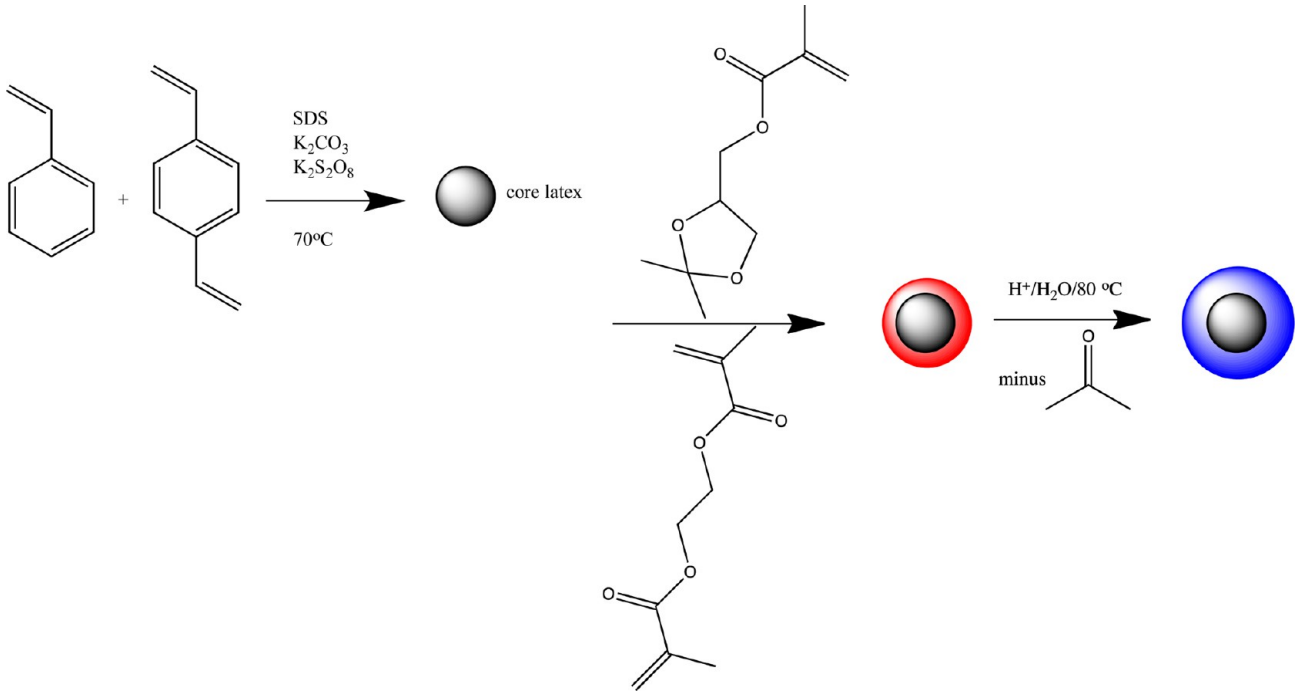

centrifuged to remove bulk water. The protein solutions were then added, and the solutions were incubated at 37 °C, pH 7.2, for 24 h. At the end of 24 h, the latexes were centrifuged, the protein solutions were removed, and the latexes were washed twice with KCl (1.0 mmol dm^{-3}). The proteins adsorbed on the particle surface were then analyzed by ζ-potential measurements.

The total protein content adsorbed to the surface of the particles was analyzed using bicinchoninic acid (BCA) assay. Following the washing stage, the protein was extracted from the surface of the CS particles using a solution of 50:49.8:0.2 water/acetonitrile/trifluoroacetic acid. A total of 1 cm^3 of this extraction solution was added to the samples, which were then incubated for 1 h at 37 °C. At the end of 1 h, the extraction solution was removed and analyzed using BCA assay.

The assay was supplied with a "working reagent" comprised of 50 parts of solution A to 1 part of solution B. A total of 100 μL of the working reagent was added to a well in a 96-well plate, and 5 μL of the sample was well mixed. The solution was incubated at 37 °C for 30 min and then cooled to room temperature. The protein content was assessed against a standard containing known amounts of Alb. The color change of this solution was measured using an absorbance at 562 nm.

Data Analysis. The particle size data were compared using two-way ANOVA with the shell composition as the column factor and the protected or deprotected nature of the shell as the row factor. Tukey's post hoc analysis was used for pairwise comparisons. A similar design was used to analyze the ζ-potential data prior to and following hydrolysis of the 1,3-dioxolane group.

The protein adsorption data were analyzed using two-way ANOVA with the shell thickness or amount of cross-linking monomer as the column factors and the applied protein concentration as the row factor. Tukey's post hoc analysis was used to compare the performances of the deprotected swollen particles to those of the cores.

Analyses were carried out without repeated measurements using model 1 (fixed effects) ANOVA.

RESULTS

Preparation of CS Particles. A core latex was produced from emulsion polymerization of styrene and DVB (Scheme 1). These latexes were colloidally stable and composed of particles of an average diameter of 64 ± 1.0 nm and a ζ potential of −47 ± 2 mV. The particles are referred to as the cores. Polymerization of GMAc and EDMA was then carried out in the presence of the core latex using the formulations shown in Table 1. The second stage, shell polymerization with GMAc and EDMA, also produced stable colloids with no significant coagulum, but the particle sizes had increased as expected. The results are summarized in Table 1.

Table 1. Particle Sizes, ζ Potentials, and Solid Contents of the Poly(styrene-*co*-DVB) Core and the Nonhydrolysed CS Particles[a]

latex	GMAc/g	EDMA/g	particle size/nm	ζ potential/mV	solid content/wt %
Cores	0	0	64 ± 3	−47 ± 2.8	21.59 ± 0.13
1,1A	2.402	0.1189	73 ± 1	−44 ± 1.5	18.40 ± 0.01
1,2A	4.8055	0.1189	77 ± 4	−40 ± 0.5	24.90 ± 0.04
1,3A	7.2083	0.1189	80 ± 2	−38 ± 0.9	24.11 ± 0.007
1,1B	2.402	0.2379	77 ± 3	−39 ± 0.3	22.10 ± 0.01
1,1C	2.402	0.3569	73 ± 2	−41 ± 0.2	22.61 ± 0.29

[a]Weights of GMAc and EDMA added to poly(stryrene-*co*-DVB) (43.5 g) dispersed in water (105 cm^3). ζ potentials were obtained at pH 7.2.

Hydrolysis of the shells was used to convert the 1,3-dioxolane groups to diol units, as shown in Scheme 2. The reaction was used to convert the hydrophobic shell into a hydrophilic water-swollen hydrogel. The progress of the series of reactions (formation of CS synthesis−hydrolysis) was followed by FTIR spectroscopy, as shown in Figure 2. The core PS particles exhibited strong peaks at 3025, 2919, 2851, 1601, 1492, 1450, 1027, 907, 756, and 688 cm^{-1}. The addition of the shell of cross-linked poly(GMAc-*co*-EDMA) produced new peaks at 1720, 1365, 1221, 1071, 741, 690, and 629 cm^{-1}. Clear diagnostic changes were observed at 1720 and 1365

DOI: 10.1021/acsami.6b15004
ACS Appl. Mater. Interfaces 2017, 9, 7577−7590

Scheme 2. Acid Hydrolysis of the Shell Polymer

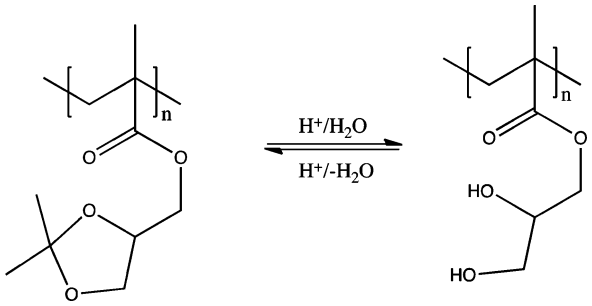

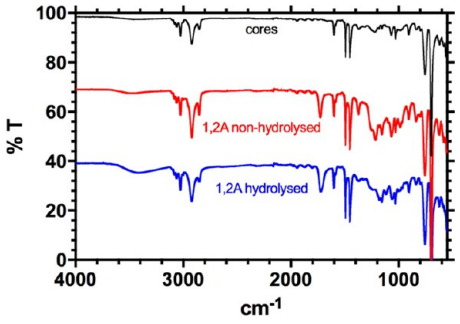

Figure 2. FTIR spectra of the core and nonhydrolyzed and hydrolyzed CS particles.

cm^{-1}, which can be assigned to the carbonyl stretch of the methacrylate group and the deformation mode of the $-CH_3$ group of 1,3-dioxolane.[61] Hydrolysis with HCl(aq) (0.1 mol dm^{-3}) caused expansion of the broad OH stretch peak around 3300 cm^{-1}, broadening of the carbonyl stretch centered at 1710 cm^{-1}, and the peak at 1365 cm^{-1} was lost. Data support hydrolysis of the 1,3-dioxolane group to produce repeat units containing a diol group (full spectra for all particles are provided in the Supporting Information).

The particle sizes of the nonhydrolyzed and hydrolyzed particles ([HCl] = 0.1 mol dm^{-3}) derived from DLS are shown in Figure 3. Deprotection of the shells by acid hydrolysis (both 0.1 mol dm^{-3}) of the 1,3-dioxolane group in each formulation provided an increase in the particle size as the shell became swollen. The data clearly showed a significant increase (**, $p < 0.01$) in the particle size between the nonhydrolyzed and hydrolyzed particles. Upon deprotection, the means of the particle distributions shifted to higher values and the distributions broadened, which reflected the dispersity in the shell compositions formed in emulsion polymerization. This hydrolysis was carried out twice at [HCl] = 0.1 or 1.0 mol dm^{-3}. Particles 1,1A, 1,2A, 1,3A 1,1B, and 1,1C were those hydrolyzed with [HCl] = 0.1 mol dm^{-3} and particles 2,1A, 2,2A, 2,3A 2,1B, and 2,1C were those obtained using [HCl] = 1.0 mol dm^{-3}. Hydrolysis with [HCl] = 1.0 mol dm^{-3} was carried out using a second batch of core and CS particles. The particle sizes of these particles are given in the Supporting Information. The increase in the particle size at [HCl] = 0.1 mol dm^{-3} suggested that little particle coagulation had occurred.

Hydrolysis with [HCl] = 1.0 mol dm^{-3} produced much larger particles, as shown in Figure 4. These data suggested that microflocculation had occurred at this pH. However, these larger CS particles remained colloidally stable.

Thus, the data showed that hydrolysis of the shells provided diol functionality within the shell, which swelled in water. The dispersions of the swollen CS particles were colloidally stable, although microflocculation produced larger particles at pH 1.0.

Dispersions of 1,1A, 1,2A, 1,3A, 1,1B, and 1,1C after hydrolysis were analyzed using the same technique and in a

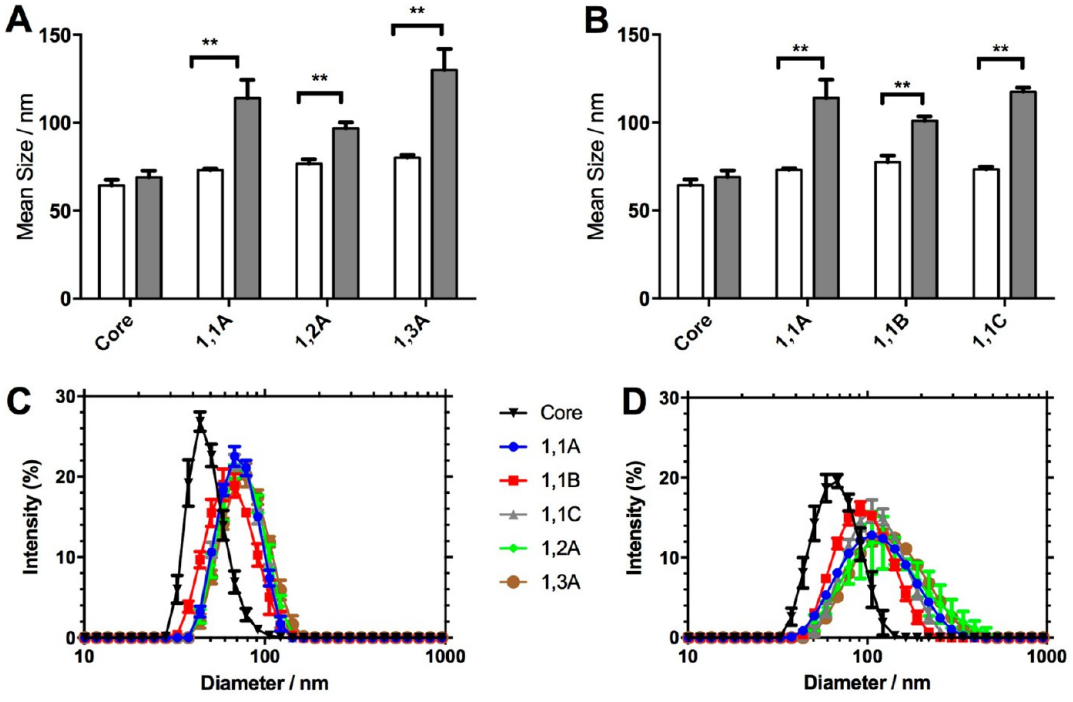

Figure 3. Particle sizes of the core and CS particles (□, nonhydrolyzed; ■, hydrolyzed) sorted by (A) increasing monomer shell feed and (B) increasing cross-linker shell feed. Significant differences are indicated as follow: ***, $p < 0.001$; **, $p < 0.01$; *, $p < 0.05$. Particle size distributions (C) of the nonhydrolyzed particles and (D) after hydrolysis.

DOI: 10.1021/acsami.6b15004
ACS Appl. Mater. Interfaces 2017, 9, 7577−7590

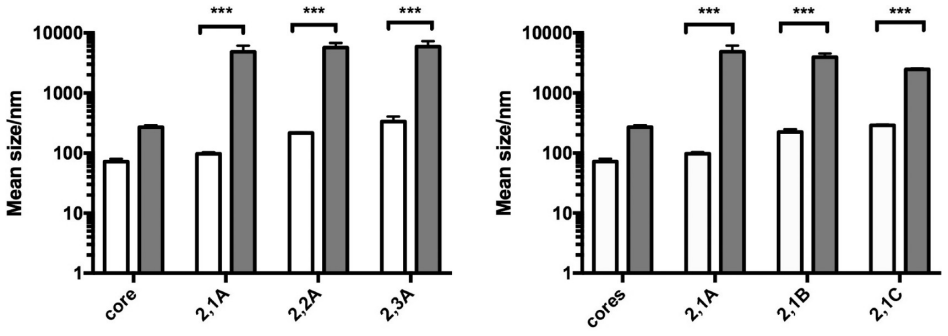

Figure 4. Mean particle sizes obtained with hydrolysis at [HCl] = 1.0 mol dm^{-3}. Significant differences are indicated as follows: ***, $p < 0.001$; **, $p < 0.01$; *, $p < 0.05$.

way equivalent to determination of the mean particle size (Figures 5 and 6). Visual inspection of the topographical images of some dried samples showed individual particles that lie in a monolayer, and no doubling up of the mean particle heights was observed. The images suggested that little flocculation had occurred in the suspension, but packing of the particles occurred upon drying. Particle sizes before hydrolysis were found to be 56 ± 1, 65 ± 1, 54 ± 2, 45 ± 1, and 49 ± 2 for 1,1A, 1,2A, 1,3A, 1,1B, and 1,1C, respectively (see the Supporting Information). These sizes were all smaller than the sizes observed via DLS measurements (see Table 1). Figures 5 and 6 show the AFM phase and height images of hydrolyzed (0.1 mol dm^{-3}) particles. Phase images are captured simultaneously with the corresponding height images. In tapping mode, the phase signal is the shift between the excitation drive frequency of the oscillating cantilever and the resulting response of the tip. Phase images are typically difficult to interpret but, in general, are related to energy dissipation between the tip and sample and also can be correlated with the adhesion, viscoelastic properties, capillary forces, and surface charges.[62] The phase signal from the spheres is lower than that found on the glass substrate, showing that, as expected, these spheres are softer and more dissipative than the glass substrate.

The measured particle diameters were 55 ± 2, 57 ± 1, 58 ± 2, 59 ± 1, and 61 ± 1 nm for 1,1A, 1,2A, 1,3A, 1,1B, and 1,1C, respectively. These data were similar to the nonhydrolyzed values, indicating deswelling of the shells upon drying. Analysis of the individual particles hydrolyzed at [HCl] = 1 mol dm^{-3} proved impossible as the particles aggregated during the drying process.

Examples of TEM images for the core and CS particles are shown in Figure 7, hydrolyzed in [HCl] = 0.1 mol dm^{-3}. The images confirmed the spherical nature of the particles. Using this technique, the average particle diameter of the cores was 46.6 ± 0.6 nm and the mean diameters of dried CS particles were 60.8 ± 0.5, 60.3 ± 5, 63.9 ± 0.8, 62.2 ± 0.7, and 67.0 ± 1.3 nm. There was no significant difference between the sizes of the CS particles in the dried form.

However, there was a significant increase ($p < 0.001$) in the mean diameter of the core compared to all of the CS particles. The data indicated that the shells have thicknesses (non-swollen) of 5−10 nm.

Protein adsorption to the particles formed by hydrolysis with [HCl] = 1.0 mol dm^{-3} was studied, and prior to these studies, the surfactant was removed by ion exchange and dialysis. Figure 8 provides ζ-potential data for the cores and hydrolyzed CS particles before and after removal of the surfactant. ANOVA showed no significant differences between the samples and cores when grouped by increasing shell monomer feed concentration ($p = 0.11$) and increasing EDMA concentration ($p = 2.11$) either before or after removal of the surfactant. However, there was a significant decrease in the ζ potential between the samples before and after purification ($p < 0.01$). After removal of the surfactant and concomitant reduction of the ζ potentials, the CS particle dispersions became less colloidally stable. However, although the particles settled, they could be easily redispersed with shaking.

Protein Adsorption. The adsorption of proteins is an important initial step in the interactions of biological milieu. The processes involved in protein adsorption to materials are complex, but some insight can be obtained by measuring both the amounts of adsorbed protein and changes in the ζ potential. On the other hand, changes in the ζ potential reflect both the amount of adsorbed protein and changes in the conformation of the protein upon adsorption. Three serum proteins (Alb, Fib, and Lys) were applied as model proteins, for blood contacting materials, at varying concentrations.

Figure 9 shows the data from total protein measurements providing adsorption isotherms expressed as the amount of protein adsorbed per unit of surface area of each of the three proteins at a range of concentrations. As a useful basis for comparisons of the behavior, Rabanal et al. recently pointed out that surface monolayers would be achieved assuming no denaturation with Alb or Lys at surface densities of 0.022 Alb nm^{-2} and 0.08 Lys nm^{-2}.[32] Similarly, solvated Fib is cylinderical with a length of 45 nm and a diameter of 9 nm.[63] This gives a surface density required to give a monolayer of 0.0025 Fib nm^{-2}

Part 1 of Figure 9 shows the Alb data. Different particles are compared to a control the core without a shell. The first observation to be made from these data is that each of the shells reduced the amount of protein adsorbed but that there were differences between the different CS particles as well. There was a substantial and significant ($p < 0.05$) difference between the amounts of protein adsorbed per unit area to the cores and each of the CS particles. The amount of Alb adsorbed to the cores did not increase as the applied concentration increased, but the amounts adsorbed were less than the amounts predicted to provide monolayer coverage of the protein in its native conformation. Each of the CS particles also adsorbed much less protein than the amounts predicted to be required to produce a monolayer. Particles 2,1A, 2,1B, and 2,1C were prepared with a constant amount of GMAc but increasing amounts of the polyfunctional monomer (EDMA). The data show that increasing the amount of EDMA led to increased levels of adsorbed protein, and in CS particles 2,1C, the

DOI: 10.1021/acsami.6b15004
ACS Appl. Mater. Interfaces 2017, 9, 7577−7590

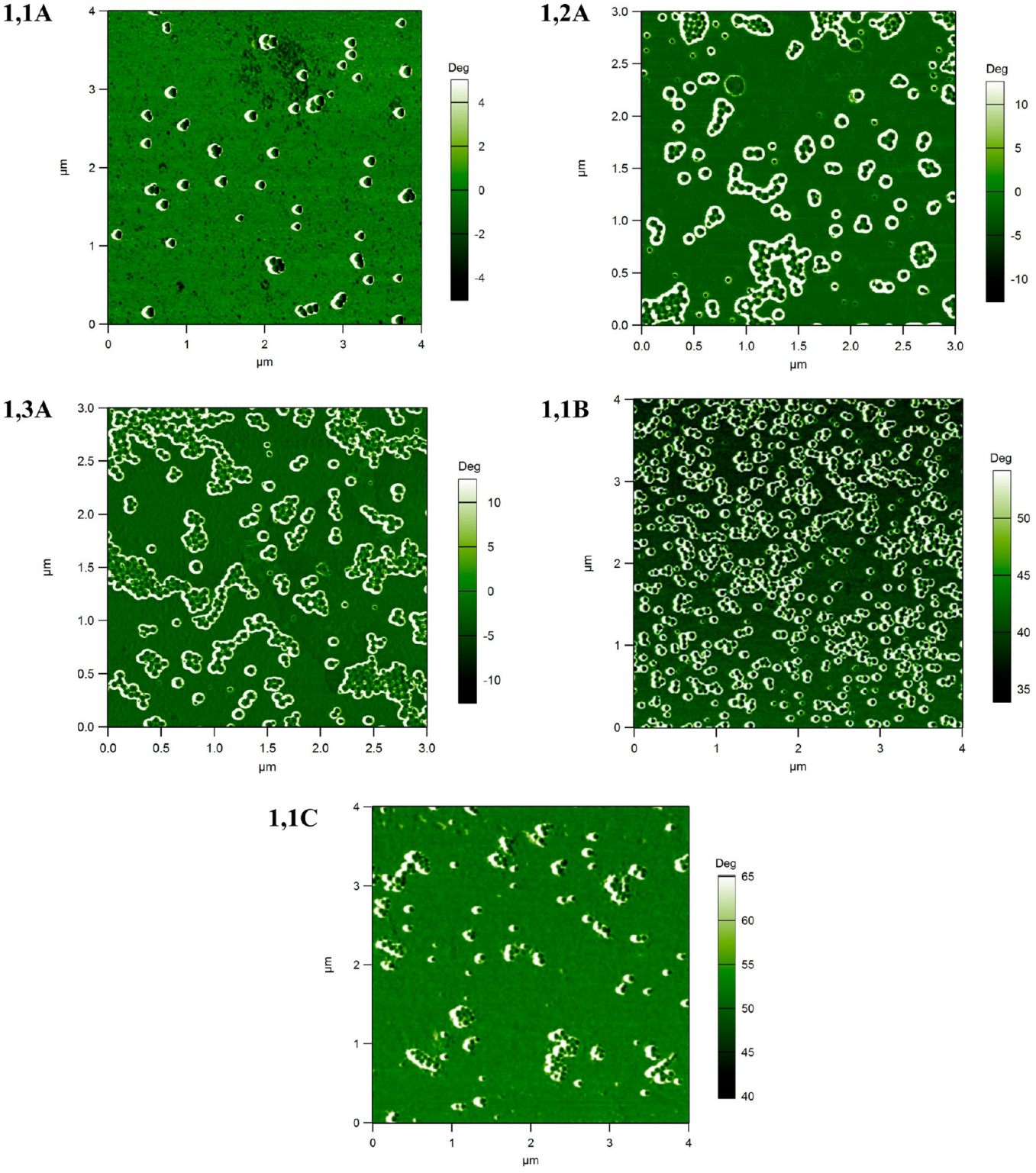

Figure 5. AFM images of dried hydrolyzed ([HCl] = 0.1 mol dm^{-3}) particles on microscope slides. 1,1A, 1,2A, 1,3A, 1,1B, and 1,1C are formulations defined in Table 1.

increase was significant ($p < 0.05$) at all concentrations of applied protein. Also, the amount adsorbed to 2,1C increased continuously as the applied concentration increased ($p < 0.05$). The series of particles 2,1A, 2,2A, and 2,3A were prepared with constant feeds of EDMA but increasing amounts of GMAc. The data show that increasing the amount of GMAc in the shell produced particles that adsorbed increased quantities of Alb. Significant changes in the amount of protein adsorbed were observed within this series of materials ($p < 0.05$), although the difference between the 2,1A and 2,1B particles was only apparent at the highest applied concentration of Alb.

Adsorption isotherms obtained following exposure to Lys are shown in part 2 of Figure 9, and the data are similar to those obtained with Alb. As in the previous data, there was a

DOI: 10.1021/acsami.6b15004
ACS Appl. Mater. Interfaces 2017, 9, 7577−7590

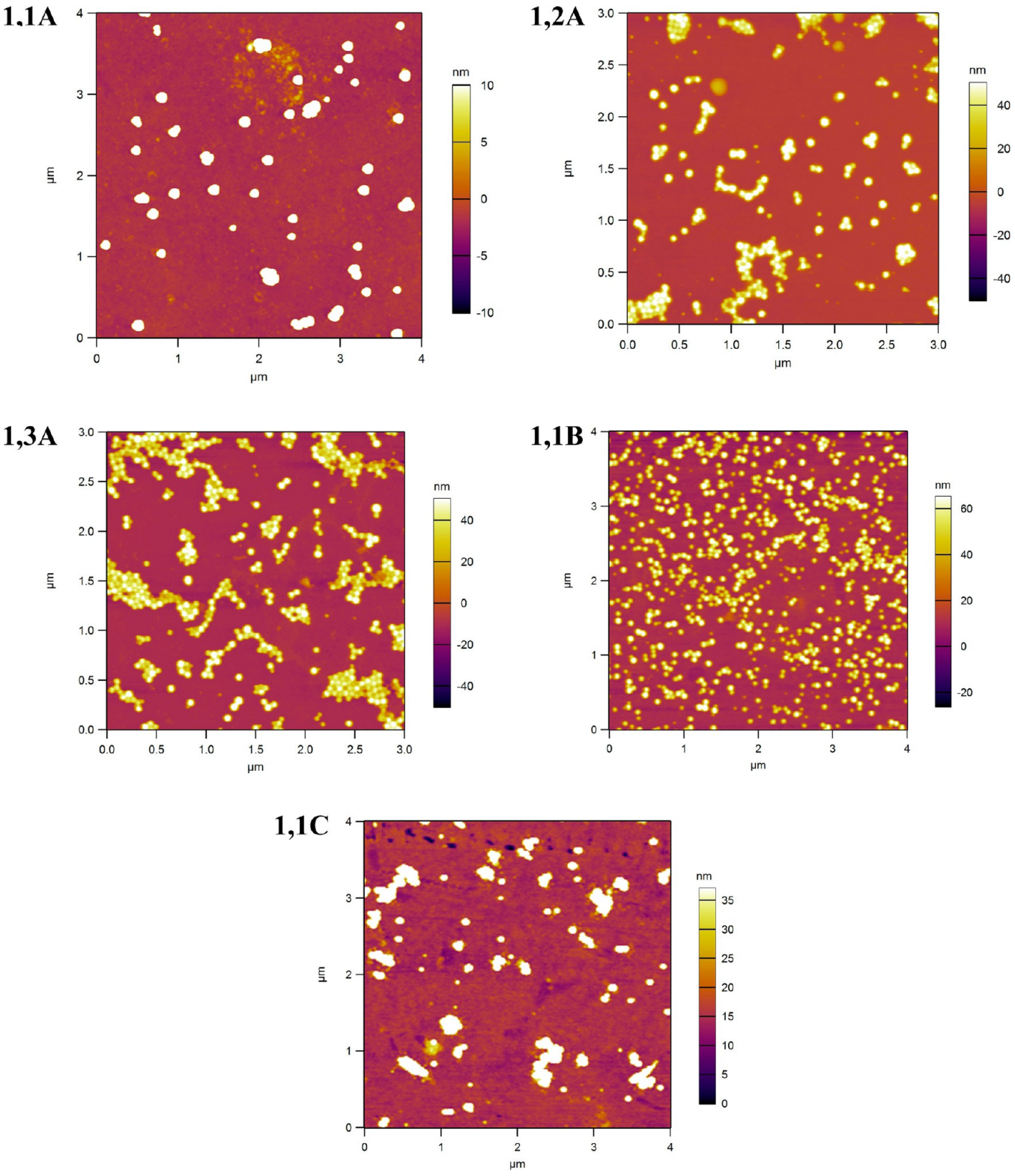

Figure 6. AFM topographical images of dried hydrolyzed ([HCl] = 0.1 mol dm^{-3}) particles on microscope slides. 1,1A, 1,2A, 1,3A, 1,1B, and 1,1C are formulations defined in Table 1.

substantial and significant ($p < 0.05$) difference between the behavior of the noncoated particles and the hydrolyzed CS particles. The trends were very similar to those observed with the data associated with Alb adsorption; formulation 2,1C adsorbed more Lys ($p < 0.05$) than the other materials, formulation 2,1A adsorbed the least, and small increases in the amounts adsorbed were seen as the fraction of EDMA or the amount of GMAc in the feed was increased. Unlike the Alb data, the amount of Lys adsorbed to the cores increased as the concentration of the applied protein increased until the amounts adsorbed approached the critical monomer layer density for this protein (0.08 molecules nm^{-2}). Importantly, the

DOI: 10.1021/acsami.6b15004
ACS Appl. Mater. Interfaces 2017, 9, 7577−7590

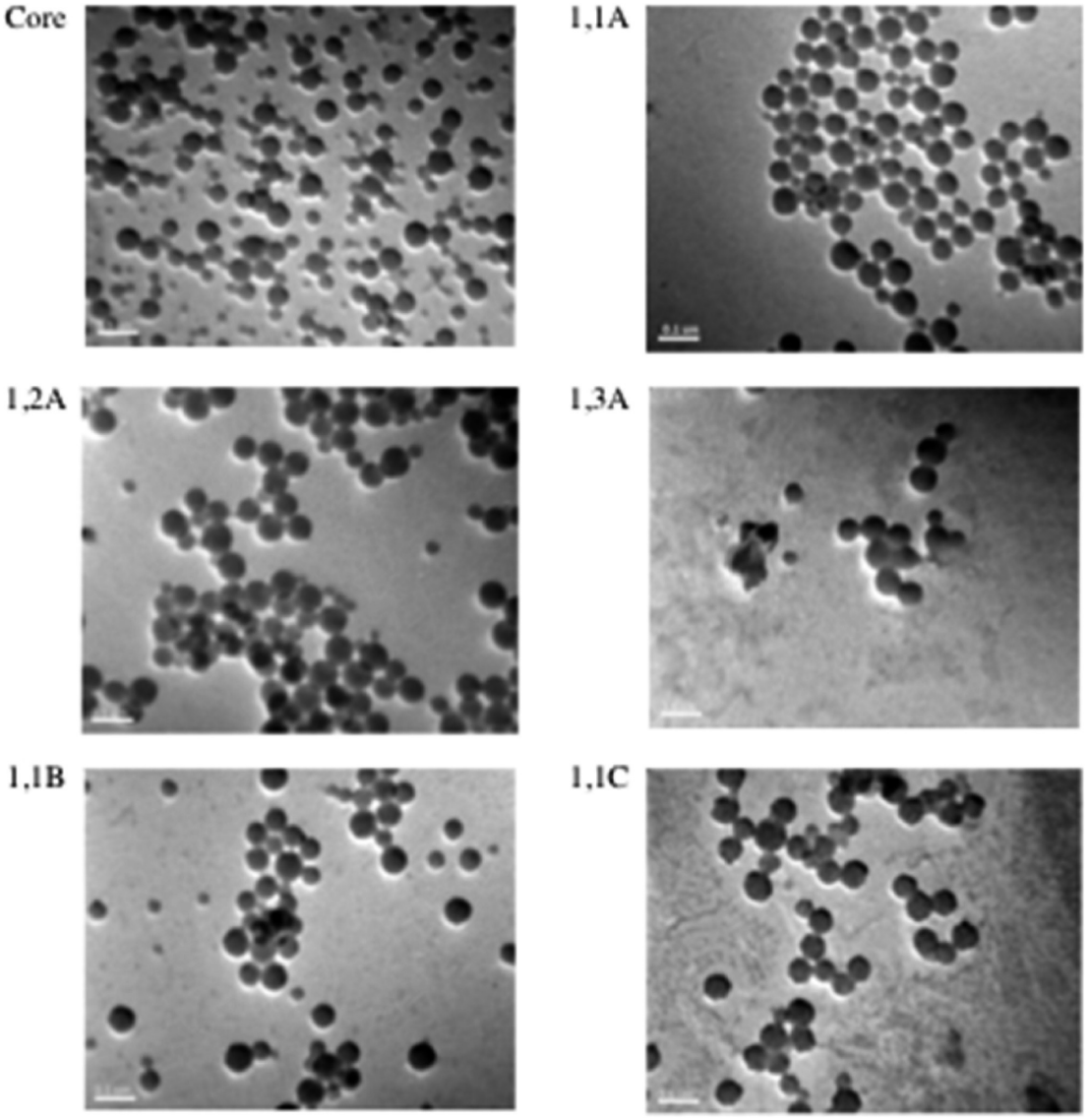

Figure 7. TEM images of hydrolyzed CS particles. 1,1A, 1,2A, 1,3A, 1,1B, and 1,1C are formulations defined in Table 1. Scale bar = 0.1 μm.

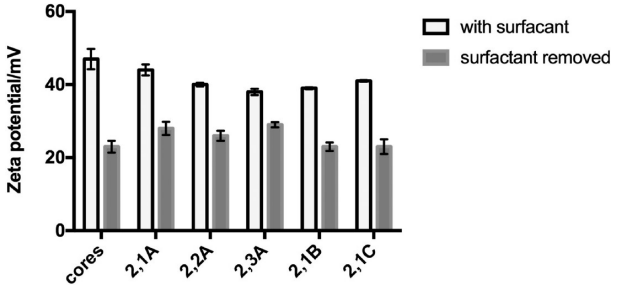

Figure 8. ζ-potential measurement (pH 7.2) derived from the cores and CS particles before and after purification. The error bars are standard errors of the mean.

amounts of Lys adsorbed to each of the CS particles were substantially lower.

Part 3 of Figure 9 shows the data obtained after exposure of the particles to Fib. The adsorption of this protein was quite different from the adsorption of Alb and Lys. First, the adsorption was more concentration-dependent, at the applied concentrations studied here, than the adsorption of Alb or Lys. Second, the amount adsorbed at saturation to the cores was substantially higher than the density required to form a monolayer. The data indicate that Fib adsorbed in multiple layers to the polystryrene cores. As with the other proteins, the amounts adsorbed to CS particles were substantially and significantly ($p < 0.01$) lower than those to the cores. The trends within the CS particles were similar to those observed with the other proteins so that Fib adsorbed to 2,1C to a significantly ($p < 0.05$) greater extent than those to the other CS particles ($p < 0.05$), and adsorption to the 2,1A particles was lower than that to any other formulation.

In general, immune cells and tissue interact in vivo with devices after they have been exposed to proteins. Adsorption of protein can provide biochemical functionalization to the interface, but also protein adsorption alters the charge state of the interface. Therefore, we examined how the protein adsorption properties of the particles changed the surface charge of the particles. The data are summarized in Figure 10, which highlights the trends in changing ζ potentials as the shell monomer concentration and shell cross-linking density are varied.

DOI: 10.1021/acsami.6b15004
ACS Appl. Mater. Interfaces 2017, 9, 7577−7590

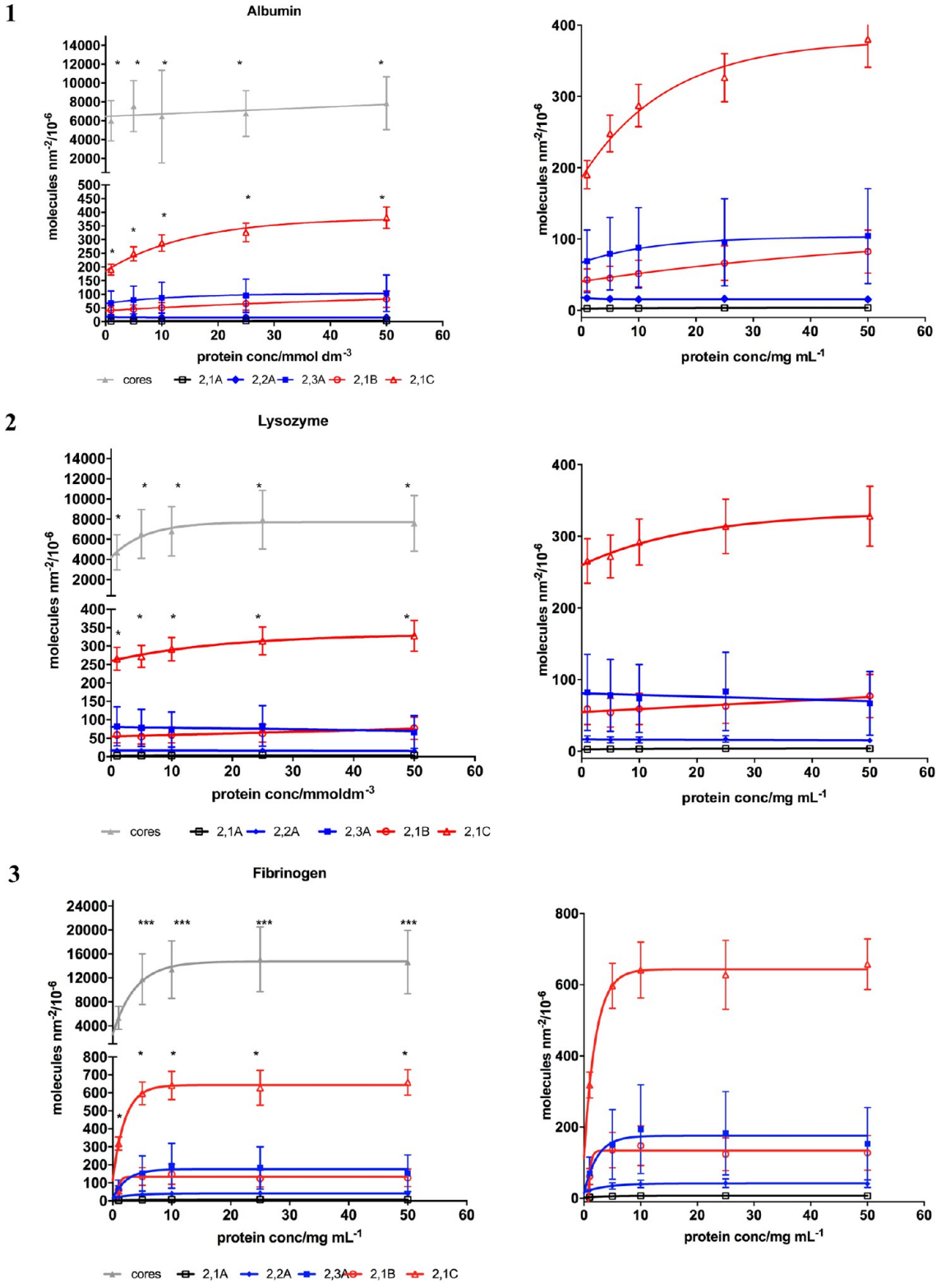

Figure 9. Protein adsorption (1, Alb; 2, Lys; 3, Fib; determined by BCA assay of proteins at varying concentrations on the core and CS particles. 2,1A (1,1A), 2,2A (1,2A), 2,3A (1,3A), 2,1B (1,1B), and 2,1C (1,1C) are derived from formulations defined in Table 1 (in parentheses) hydrolyzed at 1.0 mol dm^{-3}. Significant differences are indicated as follows: ***, $p < 0.001$; **, $p < 0.01$; *, $p < 0.05$. The error bars are standard errors of the mean.

Part 1 of Figure 10 shows the changes in the ζ potentials as a negatively charged protein, Alb, adsorbs to the shell. The data show a significant difference between the core and some of the CS particles, and there was a general increase in ζ potential after Alb adsorbed to the CS particles compared to the cores. However, a comparison of these data, using ANOVA, showed no significant differences as the concentration of the applied protein was increased. This result is in general agreement with

DOI: 10.1021/acsami.6b15004
ACS Appl. Mater. Interfaces 2017, 9, 7577−7590

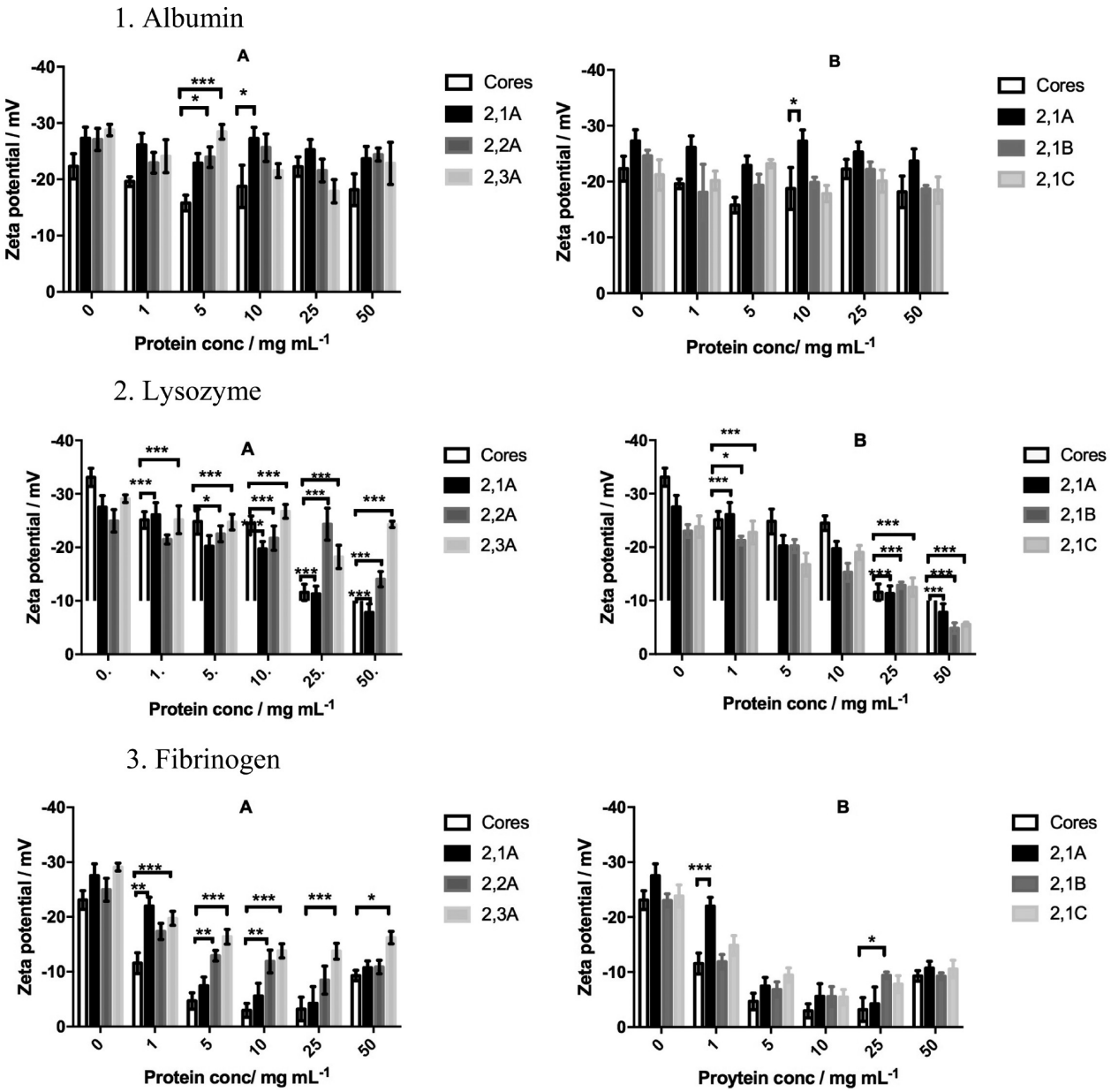

Figure 10. Variation of the ζ potential (pH 7.2) following exposure to Alb, Fib, or Lys. 2,1A (1,1A), 2,2A (1,2A), 2,3A (1,3A), 2,1B (1,1B), and 2,1C (1,1C) are derived from formulations defined in Table 1 (in parentheses) hydrolyzed at 1.0 mol dm^{-3}. Significant differences are indicated as follows: ***, $p < 0.001$; **, $p < 0.01$; *, $p < 0.05$. The error bars are standard errors of the mean.

the data shown in part 1 of Figure 10, which showed that (with the exception of the CS particles 2,1C), although the amount of protein adsorbed was below the critical amount that would be predicted to form a monolayer, increasing the concentration of protein did not result in increased adsorption.

Part 2 of Figure 10 shows how the ζ potential varied when Lys was added. Lys is an important antimicrobial peptide. We hypothesized that electrostatic interactions (a positively charged protein with a negatively charged shell) would drive increased adsorption compared to the other proteins and the small size (14307 g mol^{-1}) of Lys would allow substantial absorption into the swollen shell. Part 2A of Figure 10 shows how the performance of the particles changed as the shell monomer concentration changed and the amount of added Lys increased. ANOVA was used to assess the significant differences in the data and showed that there were no significant differences in the ζ potential between the three CS particles and the cores in the absence of Lys. However, at all concentrations of Lys, the ζ potential of the CS particles was lower than that of the cores ($p < 0.01$), and at a concentration of 25 mg mL^{-1}, the ζ potential had effectively decreased to 0 mV ($p < 0.01$). All of the CS particles maintained higher negative ζ potentials, which were in most comparisons significantly different from the cores. The results indicated that, although the core and CS particles had similar ζ potentials, initially the CS particles were substantially more resistant to the adsorption of Lys than the cores. Also, the particles prepared with the highest feed of GMAc (2,3A) maintained the initial ζ potential up to 50 mg mL^{-1} of Lys. Part 2B of Figure 10 shows the effect of changing the amount of EDMA in the polymerization feed. In the absence of Lys, there were no significant differences in the ζ potentials between the core and

DOI: 10.1021/acsami.6b15004
ACS Appl. Mater. Interfaces 2017, 9, 7577−7590

any of the CS particles. At all concentrations of Lys, the ζ potentials of the CS particles were higher than those of the cores, and at concentrations of 25 and 50 mg mL^{-1} Lys, the differences were highly significant ($p < 0.001$). There were significant differences at a concentration of 1 mg mL^{-1} also.

Clearly, the ζ potentials of these CS particles decrease substantially at concentrations of applied Lys of 25 and 50 mg mL^{-1}, but the decrease was much less than that observed on the cores. Also, at concentrations of 1 mg mL^{-1}, there was no significant decrease in the ζ potential on the CS particles, whereas the mean ζ potential of the cores decreased from −23 to −15 mV ($p < 0.01$).

The effect of the adsorption of Fib was very different, and part 3 of Figure 10 shows the data. Examination of the adsorption of this protein to the cores illustrates a complex relationship between the concentration of applied Fib and the ζ potential. The ζ potential showed a substantial and significant ($p < 0.001$) decrease at 1 mg mL^{-1} followed by smaller reductions as the applied amount of protein increased. The effects of adding the shell are quite clear in part 3A of Figure 10; at each concentration of protein, the decrease in the ζ potential was much less for the CS particles than for the cores. Each of the CS particles produced samples with decreasing ζ potential as the concentration of applied Fib increased to 25 mg mL^{-1}; then as the concentration was further increased to 50 mg mL^{-1}, the ζ potentials increased. Thus, the behavior of the CS particles in relation to changes in the concentration of this protein was similar to that observed with the cores. However, at all concentrations, the thickest shell, particles 2,3A, produced the smallest changes in the ζ potential compared to the cores, and these differences were significant at all concentrations of applied protein. Part 3A of Figure 10 also indicates that the CS particles 2,1A and 2,2A with adsorbed Fib had ζ potentials that were in each instance higher than those of the cores with adsorbed Fib. However, not all of these differences were statistically significant. Part 3B of Figure 10 shows how the ζ potential varied with the Fib concentration and the amount of EDMA in the feed. Changing the amount of EDMA in the feed alters the cross-linking density, but in this specific series, there seemed to be little effect of changing this parameter at Fib concentrations of 5 mg mL^{-1} and higher. However, exposure of Fib at a concentration of 1 mg mL^{-1} to the CS particles with the lowest nominal cross-linking density (2,1A) showed no significant change from the sample not exposed to Fib. The mean ζ potential of this particle was maintained in the presence of protein at this concentration, and it was significantly higher than values derived from the core or the two other CS particles ($p < 0.05$).

DISCUSSION

The use of sequential emulsion polymerization has allowed for the synthesis of CS polystyrene−PGMAc particles, which were then hydrolyzed to provide CS particles with cross-linked hydrogel shells. The three-step preparation produced dispersions of spherical particles that were free of surfactant, following ion exchange and dialysis. Previously, we had shown that hydrogel sheets composed of GMA cross-linked with EDMA did not provide substrates for the adhesion of human adherent cells unless either hydrophobic segments or cell-adhesion-promoting peptides were added. High-water-content GMA hydrogels were also shown not to activate immune cells (murine peritoneal macrophages) and to be resistant to protein adsorption. The work in this area supported the data showing that noncharged hydrogels were non-cell-adhesive[35,36] and protein-resistant[43,44,64] and do not initiate an immune response.[41] CS particles with GMA shells would thus be useful as stealth particles that could be used to deliver therapeutic compounds. Also, after coagulation, aggregates of particles can be used to form porous materials of use as scaffolds for tissue engineering.[65] The thickness of the shell and the degrees of swelling affect how the particles interact with biological milieu. However, adding a more substantial hydrogel shell to a hydrophobic particle is nontrivial. Here we showed that this could be achieved with a monomer that had an appropriate solubility in water to facilitate conventional emulsion polymerization followed by modification of the repeat units to provide a hydrophilic water-swollen shell. To illustrate this approach, we added the shell to a polystyrene core.

The key first process that occurs when materials interact with biological media is protein adsorption, and here we examined the adsorption of three key proteins of relevance to the in vivo use of these particles. There were clear effects of adding the GMA shells. In this case, protein adsorption was reduced on the CS particles, but the importance of considering the shell thickness and cross-linking (swelling) was indicated by the differences between the variously formulated particles. Importantly, these parameters are easily varied using the synthetic methodology reported here, and in future work, fully optimized CS particles will be further disclosed. Alb is typically present in vivo in blood at concentrations of 35−53 mg mL^{-1}.[66] Lys can be present in blood at around 10^{-3} mg mL^{-1},[67] but in tears, the normal level is 1−2 mg mL^{-1}.[68] In blood, Fib is present at concentrations of 1.5−4.5 mg mL^{-1}.[69] Therefore, the protein adsorption data presented here are relevant to the observed in vivo concentrations of these proteins, and similar particles with these hydrogel shells, especially those based on formulation 1A, would be expected to be resistant to protein adsorption in vivo.

CONCLUSION

Here we show how CS particles with a model hydrophobic polymer core (polystyrene) can be prepared by sequential emulsion polymerization followed by hydrolysis of groups within the shell to give a glycol functional shell. The swollen particles were shown to adsorb less protein than the hydrophobic core, and the performance in this respect was dependent on the composition of the shell.

ASSOCIATED CONTENT

Supporting Information

The Supporting Information is available free of charge on the ACS Publications website at DOI: 10.1021/acsami.6b15004.

AFM and TEM images of nonhydrolyzed particles, gravimetric solid content, NMR and mass spectral data for GMAc, FTIR data of all particles, and correlograms of the DLS data (PDF)

AUTHOR INFORMATION

Corresponding Author

*E-mail: s.rimmer@bradford.ac.uk.

ORCID

Thomas Swift: 0000-0002-8616-8458

Stephen Rimmer: 0000-0002-1048-1974

DOI: 10.1021/acsami.6b15004
ACS Appl. Mater. Interfaces 2017, 9, 7577−7590

Author Contributions

The manuscript was written through contributions of all authors. All authors have given approval to the final version of the manuscript.

Notes

The authors declare no competing financial interest.

■ ACKNOWLEDGMENTS

The authors are grateful to EPSRC for providing a studentship for Andrew MacKenzie and to the MRC (MR/N501888/2) for providing a postdoctoral fellowship for Richard Hoskins. We are also grateful to Graeme Dean for technical support.

■ REFERENCES

(1) Langer, R. *Science* **2001**, *293*, 58−59.
(2) Laroui, H.; Dalmasso, G.; Nguyen, H. T. T.; Yan, Y. T.; Sitaraman, S. V.; Merlin, D. Drug-Loaded Nanoparticles Targeted to the Colon with Polysaccharide Hydrogel Reduce Colitis in a Mouse Model. *Gastroenterology* **2010**, *138*, 843−853.
(3) Paulino, A. T.; Guilherme, M. R.; Mattoso, L. H. C.; Tambourgi, E. B. Smart Hydrogels Based on Modified Gum Arabic as a Potential Device for Magnetic Biomaterial. *Macromol. Chem. Phys.* **2010**, *211*, 1196−1205.
(4) Lim, S. M.; Oh, S. H.; Lee, H. H.; Yuk, S. H.; Im, G. I.; Lee, J. H. Dual Growth Factor-releasing Nanoparticle/Hydrogel System for Cartilage Tissue Engineering. *J. Mater. Sci.: Mater. Med.* **2010**, *21*, 2593−2600.
(5) Platt, L.; Kelly, L.; Rimmer, S. Controlled Delivery of Cytokine Growth Factors Mediated by Core-Shell Particles with Poly-(acrylamidomethylpropane sulphonate) Shells. *J. Mater. Chem. B* **2014**, *2*, 494−501.
(6) Chatterjee, K.; Sarkar, S.; Jagajjanani Rao, K.; Paria, S. Core/shell Nanoparticles in Biomedical Applications. *Adv. Colloid Interface Sci.* **2014**, *209*, 8−39.
(7) Goldberg, M.; Langer, R.; Jia, X. Q. Nanostructured Materials for Applications in Drug Delivery and Tissue Engineering. *J. Biomater. Sci., Polym. Ed.* **2007**, *18*, 241−268.
(8) Hoffman, A. S. Applications of Thermally Reversible Polymers and Hydrogels in Therapeutics and Diagnostics. *J. Controlled Release* **1987**, *6*, 297−305.
(9) Lv, S.; Liu, L.; Yang, W. Preparation of Soft Hydrogel Nanoparticles with PNIPAm Hair and Characterization of Their Temperature-Induced Aggregation. *Langmuir* **2010**, *26*, 2076.
(10) Haag, R. Supramolecular Drug-Delivery Systems Based on Polymeric Core−Shell Architectures. *Angew. Chem., Int. Ed.* **2004**, *43*, 278−282.
(11) Bonner, D. K.; Leung, C.; Chen-Liang, J.; Chingozha, L.; Langer, R.; Hammond, P. T. Intracellular Trafficking of Polyamido-amine−Poly(ethylene glycol) Block Copolymers in DNA Delivery. *Bioconjugate Chem.* **2011**, *22*, 1519−1525.
(12) Asselin, J.; Roy, C.; Boudreau, D.; Messaddeq, Y.; Bouchareb, R.; Mathieu, P. Supported Core-shell Nanobiosensors for Quantitative Fluorescence Imaging of Extracellular pH. *Chem. Commun.* **2014**, *50*, 13746−13749.
(13) Yang, S. B.; Wu, T. F.; Zhao, X. H.; Li, X. F.; Tan, W. B. The Optical Property of Core-Shell Nanosensors and Detection of Atrazine Based on Localized Surface Plasmon Resonance (LSPR). *Sensors* **2014**, *14*, 13273−13284.
(14) Yi, R.; Ye, G.; Pan, D.; Wu, F.; Wen, M.; Chen, J. Novel Core-Shell Structured Superparamagnetic Microspheres Decorated with Macrocyclic Host Molecules for Specific Recognition and Magnetic Removal of Pb(II). *J. Mater. Chem. A* **2014**, *2*, 6840−6846.
(15) Zang, W.; Nie, Y.; Zhu, D.; Deng, P.; Xing, L.; Xue, X. Core−Shell In2O3/ZnO Nanoarray Nanogenerator as a Self-Powered Active Gas Sensor with High H2S Sensitivity and Selectivity at Room Temperature. *J. Phys. Chem. C* **2014**, *118*, 9209−9216.
(16) Pang, Y.; Rong, Z.; Wang, J.; Xiao, R.; Wang, S. A Fluorescent Aptasensor for H5N1 Influenza Virus Detection Based-on the Core−Shell Nanoparticles Metal-Enhanced fluorescence (MEF). *Biosens. Bioelectron.* **2015**, *66*, 527−532.
(17) Majewski, A. P.; Stahlschmidt, U.; Jérôme, V.; Freitag, R.; Müller, A. H. E.; Schmalz, H. PDMAEMA-Grafted Core−Shell−Corona Particles for Nonviral Gene Delivery and Magnetic Cell Separation. *Biomacromolecules* **2013**, *14*, 3081−3090.
(18) Verma, N. K.; Crosbie-Staunton, K.; Satti, A.; Gallagher, S.; Ryan, K. B.; Doody, T.; McAtamney, C.; MacLoughlin, R.; Galvin, P.; Burke, C. S.; Volkov, Y.; Gun'ko, Y. K. Magnetic Core-shell Nanoparticles for Drug Delivery by Nebulization. *J. Nanobiotechnol.* **2013**, *11*, 1.
(19) Darwish, M. S. A.; Kunz, U.; Peuker, U. Preparation and Catalytic Use of Platinum in Magnetic Core/Shell Nanocomposites. *J. Appl. Polym. Sci.* **2013**, *129*, 1806−1811.
(20) Pelton, R.; Hoare, T., Microgels and Their Synthesis: An Introduction. *Microgel Suspensions*; Wiley-VCH Verlag GmbH & Co. KGaA: Weinheim, Germany, 2011; pp 1−32.
(21) Rimmer, S.; Mohd Ramli, A. N.; Lefèvre, S. Preparation of Polystyrene-poly (styrene-g-N-isopropylacrylamide) Core-Shell Particles: Copolymerization of Oligo (N-isopropylacrylamide) Macromonomers and Styrene onto Polystyrene Seed Particles and Stability of the Resultant Particles. *Polymer* **1996**, *37*, 4135−4139.
(22) Atkin, R.; Bradley, M.; Vincent, B. Core-Shell Particles Having Silica Cores and pH-Responsive Poly(vinylpyridine) Shells. *Soft Matter* **2005**, *1*, 160−165.
(23) Yun, Y.; Li, H.; Ruckenstein, E. Hydrophobic Core/Hydrophilic Shell Amphiphilic Particles. *J. Colloid Interface Sci.* **2001**, *238*, 414−419.
(24) Hoare, T.; Pelton, R. Highly pH and Temperature Responsive Microgels Functionalized with Vinylacetic Acid. *Macromolecules* **2004**, *37*, 2544−2550.
(25) Liu, S.; Weaver, J. V. M; Save, M.; Armes, S. P. Synthesis of pH-Responsive Shell Cross-Linked Micelles and Their Use as Nanoreactors for the Preparation of Gold Nanoparticles. *Langmuir* **2002**, *18*, 8350−8357.
(26) Chen, X. Y.; Armes, S. P.; Greaves, S. J.; Watts, J. F. Synthesis of Hydrophilic Polymer-Grafted Ultrafine Inorganic Oxide Particles in Protic Media at Ambient Temperature via Atom Transfer Radical Polymerization: Use of an Electrostatically Adsorbed Polyelectrolytic Macroinitiator. *Langmuir* **2004**, *20*, 587−595.
(27) Duracher, D.; Sauzedde, F.; Elaissari, A.; Perrin, A.; Pichot, C. Cationic Amino-Containing N-isopropyl- acrylamide−styrene Copolymer Latex Particles: 1-Particle Size and Morphology vs. Polymerization Process. *Colloid Polym. Sci.* **1998**, *276*, 219−231.
(28) Duracher, D.; Sauzedde, F.; Elaïssari, A.; Pichot, C.; Nabzar, L. Cationic Amino-containing N-isopropyl- Acrylamide-Styrene Copolymer Particles: 2-Surface and Colloidal Characteristics. *Colloid Polym. Sci.* **1998**, *276*, 920−929.
(29) Nabzar, L.; Duracher, D.; Elaïssari, A.; Chauveteau, G.; Pichot, C. Electrokinetic Properties and Colloidal Stability of Cationic Amino-Containing N-Isopropylacrylamide−Styrene Copolymer Particles Bearing Different Shell Structures. *Langmuir* **1998**, *14*, 5062−5069.
(30) Hellweg, T.; Dewhurst, C. D.; Eimer, W.; Kratz, K. PNIPAM-co-polystyrene Core−Shell Microgels: Structure, Swelling Behavior, and Crystallization. *Langmuir* **2004**, *20*, 4330−4335.
(31) Pfaff, A.; Shinde, V. S.; Lu, Y.; Wittemann, A.; Ballauff, M.; Müller, A. H. E. Glycopolymer-Grafted Polystyrene Nanospheres. *Macromol. Biosci.* **2011**, *11*, 199−210.
(32) Rabanel, J.-M.; Faivre, J.; Tehrani, S. F.; Lalloz, A.; Hildgen, P.; Banquy, X. Effect of the Polymer Architecture on the Structural and Biophysical Properties of PEG−PLA Nanoparticles. *ACS Appl. Mater. Interfaces* **2015**, *7*, 10374−10385.
(33) Feeney, O. M.; Williams, H. D.; Pouton, C. W.; Porter, C. J. H. 'Stealth' Lipid-Based Formulations: Poly(ethylene glycol)-Mediated Digestion Inhibition Improves Oral Bioavailability of a Model Poorly Water Soluble Drug. *J. Controlled Release* **2014**, *192*, 219−227.

DOI: 10.1021/acsami.6b15004
ACS Appl. Mater. Interfaces 2017, 9, 7577−7590

(34) Moghimi, S. M.; Farhangrazi, Z. S. Nanoparticles in Medicine: Nanoparticle Engineering for Macrophage Targeting and Nanoparticles that Avoid Macrophage Recognition. In *Nanoparticles and the Immune System*; Boraschi, D., Duschl, A., Eds.; Academic Press: San Diego, CA, 2014; Chapter 6, pp 77−89.
(35) Mann, A.; Tighe, B. Contact Lens Interactions with the Tear Film. *Exp. Eye Res.* **2013**, *117*, 88−98.
(36) Haigh, R.; Fullwood, N.; Rimmer, S. Synthesis and Properties of Amphiphilic Networks 2: A Differential Scanning Calorimetric Study of Poly(dodecyl methacrylate-stat-2,3 propandiol-1-methacrylate-stat-ethandiol dimethacrylate) Networks and Adhesion and Spreading of Dermal Fibroblasts on these Materials. *Biomaterials* **2002**, *23*, 3509−3516.
(37) Sun, Y.; Collett, J.; Fullwood, N. J.; Mac Neil, S.; Rimmer, S. Culture of Dermal Fibroblasts and Protein Adsorption on Block Conetworks of Poly(butyl methacrylate-block-(2,3 propandiol-1-methacrylate-stat-ethandiol dimethacrylate)). *Biomaterials* **2007**, *28*, 661−670.
(38) Rimmer, S.; Johnson, C.; Zhao, B.; Collier, J.; Gilmore, L.; Sabnis, S.; Wyman, P.; Sammon, C.; Fullwood, N. J.; MacNeil, S. Epithelialization of Hydrogels Achieved by Amine Functionalization and Co-culture with Stromal cells. *Biomaterials* **2007**, *28*, 5319−5331.
(39) Hassan, E.; Deshpande, P.; Claeyssens, F.; Rimmer, S.; Macneil, S. Amine Functional Hydrogels as Selective Substrates for Corneal Epithelialization. *Acta Biomater.* **2014**, *10*, 3029−3037.
(40) Perlin, L.; MacNeil, S.; Rimmer, S. Cell Adhesive Hydrogels Synthesized by Copolymerization of Arg-protected Gly-Arg-Gly-Asp-Ser Methacrylate Monomers and Enzymatic deprotection. *Chem. Commun.* **2008**, 5951−5953.
(41) Rimmer, S.; Wilshaw, S. P.; Pickavance, P.; Ingham, E. Cytocompatibility of Poly(1,2 propandiol methacrylate) Copolymer Hydrogels and Conetworks with or without Alkyl Amine Functionality. *Biomaterials* **2009**, *30*, 2468−2478.
(42) Gao, H.; Lu, X.; Ma, Y.; Yang, Y.; Li, J.; Wu, G.; Wang, Y.; Fan, Y.; Ma, J. Amino Poly(glycerol methacrylate)s for Oligonucleic Acid Delivery with Enhanced Transfection Efficiency and Low Cytotoxicity. *Soft Matter* **2011**, *7*, 9239−9247.
(43) Robert-Nicoud, G.; Evans, R.; Vo, C.-D.; Cadman, C. J.; Tirelli, N. Synthesis, Self-assembly and (absence of) Protein Interactions of Poly(glycerol methacrylate)-Silicone Macro-amphiphiles. *Polym. Chem.* **2013**, *4*, 3458−3470.
(44) Patrucco, E.; Ouasti, S.; Vo, C. D.; De Leonardis, P.; Pollicino, A.; Armes, S. P.; Scandola, M.; Tirelli, N. Surface-Initiated ATRP Modification of Tissue Culture Substrates: Poly(glycerol monomethacrylate) as an Antifouling Surface. *Biomacromolecules* **2009**, *10*, 3130−3140.
(45) Beinert, G.; Hild, G.; Rempp, P. Préparation, Polymérisation et Réticulation du Méthacrylate de (diméthyl-2,2 dioxolann-1,3 yle-4) méthyle. Hydrolyse des Polymères Obtenus. *Makromol. Chem.* **1974**, *175*, 2069−2077.
(46) Mori, H.; Hirao, A.; Nakahama, S. Protection and Polymerization of Functional Monomers. 21. Anionic Living Polymerization of (2,2-dimethyl-1,3-dioxolan-4-yl)methyl methacrylate. *Macromolecules* **1994**, *27*, 35−39.
(47) Liu, F.; Liu, G. Poly(solketal methacrylate)-block-poly(2-cinnamoyloxyethyl methacrylate)-block-poly(allyl methacrylate): Synthesis and Micelle Formation. *Macromolecules* **2001**, *34*, 1302−1307.
(48) Cai-Yuan, P.; Lei, T.; De-Cheng, W. Synthesis and Characterizations of the Four-armed Amphiphilic Block Copolymer [Poly(2,3-dihydroxypropyl acrylate)-block-poly(methyl acrylate)]. *J. Polym. Sci., Part A: Polym. Chem.* **2001**, *39*, 3062−3072.
(49) Zhang, Z.; Liu, G.; Bell, S. Synthesis of Poly(solketal methacrylate)-block-poly(2-(dimethylamino)ethyl methacrylate) and Preparation of Nanospheres with Cross-linked Shells. *Macromolecules* **2000**, *33*, 7877−7883.
(50) Carter, S.; Rimmer, S.; Sturdy, A.; Webb, M. Highly Branched Stimuli Responsive poly[(N-isopropyl acrylamide)-co-(1,2- propandiol-3-methacrylate)]s with Protein Binding Functionality. *Macromol. Biosci.* **2005**, *5*, 373−378.
(51) Thompson, K. L.; Armes, S. P.; York, D. W.; Burdis, J. A. Synthesis of Sterically-Stabilized Latexes Using Well-Defined Poly(glycerol monomethacrylate) Macromonomers. *Macromolecules* **2010**, *43*, 2169−2177.
(52) Cunningham, V. J.; Alswieleh, A. M.; Thompson, K. L.; Williams, M.; Leggett, G. J.; Armes, S. P.; Musa, O. M. Poly(glycerol monomethacrylate)−Poly(benzyl methacrylate) Diblock Copolymer Nanoparticles via RAFT Emulsion Polymerization: Synthesis, Characterization, and Interfacial Activity. *Macromolecules* **2014**, *47*, 5613−5623.
(53) Chambon, P.; Blanazs, A.; Battaglia, G.; Armes, S. P. Facile Synthesis of Methacrylic ABC Triblock Copolymer Vesicles by RAFT Aqueous Dispersion Polymerization. *Macromolecules* **2012**, *45*, 5081−5090.
(54) Schmidt, V.; Borsali, R.; Giacomelli, C. Aggregation of a Versatile Triblock Copolymer into pH-Responsive Cross-Linkable Nanostructures in Both Organic and Aqueous Media. *Langmuir* **2009**, *25*, 13361−13367.
(55) Sato, T.; Tsuji, S.; Kawagauchi, H. Preparation of Functional Nanoparticles by Assembling Block Copolymers Formed by Living Radical Polymerization. *Ind. Eng. Chem. Res.* **2008**, *47*, 6358−6361.
(56) Amado, E.; Augsten, C.; Mäder, K.; Blume, A.; Kressler, J. Amphiphilic Water Soluble Triblock Copolymers Based on Poly(2,3-dihydroxypropyl methacrylate) and Poly(propylene oxide): Synthesis by Atom Transfer Radical Polymerization and Micellization in Aqueous Solutions. *Macromolecules* **2006**, *39*, 9486−9496.
(57) Pilon, L. N.; Armes, S. P.; Findlay, P.; Rannard, S. P. Synthesis and Characterisation of New Shell Cross-linked Micelles with Amine-functional Coronas. *Eur. Polym. J.* **2006**, *42*, 1487−1498.
(58) Pilon, L. N.; Armes, S. P.; Findlay, P.; Rannard, S. P. Synthesis and Characterization of Shell Cross-Linked Micelles with Hydroxy-Functional Coronas: A Pragmatic Alternative to Dendrimers? *Langmuir* **2005**, *21*, 3808−3813.
(59) Suzuki, D.; Yamagata, T.; Murai, M. Multilayered Composite Microgels Synthesized by Surfactant-Free Seeded Polymerization. *Langmuir* **2013**, *29*, 10579−10585.
(60) Ma, Y.; Gao, H.; Gu, W.; Yang, Y.-W.; Wang, Y.; Fan, Y.; Wu, G.; Ma, J. Carboxylated Poly(glycerol methacrylate)s for Doxorubicin Delivery. *Eur. J. Pharm. Sci.* **2012**, *45*, 65−72.
(61) Tipson, R. S.; Isbell, H. S.; Stewart, J. E. Infrared Absorption Spectra of Some Cyclic Acetals of Sugars. *J. Res. Natl. Bur. Stand.* **1959**, *62*, 257−282.
(62) Stark, M.; Möller, C.; Müller, D. J.; Guckenberger, R. From Images to Interactions: High-Resolution Phase Imaging in Tapping-Mode Atomic Force Microscopy. *Biophys. J.* **2001**, *80*, 3009−3018.
(63) Bachmann, L.; Schmitt-Fumain, W. W.; Hammel, R.; Lederer, K. Size and Shape of Fibrinogen, 1. Electron Microscopy of the Hydrated Molecule. *Makromol. Chem.* **1975**, *176*, 2603−2618.
(64) Haigh, R.; Rimmer, S.; Fullwood, N. J. Synthesis and Properties of Amphiphilic Networks. 1: The Effect of Hydration and Polymer Composition on the Adhesion of Immunoglobulin-G to Poly(laurylmethacrylate-stat-lycerolmonomethacrylate-stat-ethylene-glycol-dimethacrylate) Networks. *Biomaterials* **2000**, *21*, 735−739.
(65) Lapworth, J. W.; Hatton, P. V.; Goodchild, R. L.; Rimmer, S. Thermally Reversible Colloidal Gels for Three-dimensional Chondrocyte Culture. *J. R. Soc., Interface* **2012**, *9*, 362−375.
(66) Rodríguez-Segade, S.; Rodríguez, J.; Mayan, D.; Camiña, F. Plasma Albumin Concentration Is a Predictor of HbA1c Among Type 2 Diabetic Patients, Independently of Fasting Plasma Glucose and Fructosamine. *Diabetes Care* **2005**, *28*, 437−439.
(67) Torsteinsdóttir, I.; Håkansson, L.; Hällgren, R.; Gudbjörnsson, B.; Arvidson, N.-G.; Venge, P. Serum Lysozyme: a Potential Marker of Monocyte/macrophage Activity in Rheumatoid Arthritis. *Rheumatology* **1999**, *38*, 1249−1254.
(68) Sen, D. K.; Sarin, G. S. Biological Variations of Lysozyme Concentration in the Tear Fluids of Healthy Persons Br. *Br. J. Ophthalmol.* **1986**, *70*, 246−248.
(69) Kamath, S.; Lip, G. Y. H. Fibrinogen: Biochemistry, Epidemiology and Determinants. *QJM* **2003**, *96*, 711−729.

DOI: 10.1021/acsami.6b15004
ACS Appl. Mater. Interfaces 2017, 9, 7577−7590